Multi-wavelength, Tabletop EUV Microscope

Kenneth C. Johnson kjinnovation@earthlink.net 12/21/2015

Abstract

A compact and inexpensive EUV source using high harmonic generation can provide illumination for a tabletop EUV microscope, but such microscopes typically use only one of the source's available harmonic wavelengths. This paper outlines a microscopy system that focuses multiple harmonic wavelengths onto distinct, spatially-separated focal spots on an inspection sample, which is scanned to generate multi-spectral, diffraction-limited EUV images of the sample. The system uses diffraction optics to separate the EUV harmonics and also to separate the source's IR wavelength out of the EUV illumination.

1. Introduction

High-harmonic generation (HHG) sources generate extreme ultraviolet (EUV) radiation by stimulating atomic emission of harmonics of a fundamental infrared (IR) laser wavelength. For a laser wavelength λ, harmonic wavelengths λ / m can be generated from a monatomic gas for odd-numbered integers m. One or more such wavelengths can be used to provide illumination for an EUV microscope.

Two examples of EUV microscopes using HHG sources are described in Ref's. 1 and 2. These systems use only one wavelength harmonic from the HHG source, but an alternative imaging technique, "multiplexed ptychography" [Ref. 3], would be able to make efficient use of multiple harmonic wavelengths. This technique does not require any imaging optics between the inspection sample and the detector; it is able to construct a detailed image just from far-field diffraction patterns collected as the sample is scanned across a stationary illumination pattern. It does require illumination optics to separate the EUV harmonics into distinct, spectrally pure and spatially separated illumination spots. But the method is not significantly limited by optical aberrations in the illumination because it is able to reconstruct the illumination pattern along with the sample image.

This paper outlines an optical mechanism for separating the HHG source's EUV harmonics into distinct foci on a focal plane, and also for separating the drive laser IR from the EUV. (The IR can be many orders of magnitude more intense than the EUV.) The EUV is spectrally dispersed by a phase-Fresnel diffraction grating, which also separates most of the IR from the EUV. However, aperture diffraction scatters some of the IR power across the EUV foci. The IR diffraction tails are eliminated by forming the EUV-dispersing grating on top of a binary-optic surface topology, which creates an IR diffraction null along a nodal line covering the EUV foci.

2. System Configuration

Figure 1 schematically illustrates a multi-wavelength EUV microscope. A diffraction grating is used to separate the HHG source's EUV harmonics and also to separate the drive

laser's IR wavelength out of the EUV illumination. A phase-Fresnel grating can be used to channel most of the EUV energy into a spectrally dispersed first diffraction order, while the IR is substantially unaffected by the grating. A grazing-incidence focusing mirror condenses the EUV harmonics and IR to distinct, spatially separated foci on a focal plane where the EUV harmonics can be isolated by a slit aperture or individual pinhole apertures. (The mirror is illustrated schematically as a singlet element in Figure 1, but in practice one of the Wolter-type doublet configurations may be used. [Ref. 4]) A second grazing-incidence focusing mirror images the filtered EUV foci onto an inspection sample. (This mirror could also be a Wolter-type doublet.) A detector array collects the sample-scattered EUV radiation as the sample is scanned.

The grating is illustrated as a transmission element in Figure 1, but the system could alternatively use a reflective grating such as a grazing-incidence ruthenium reflector or a near-normal-incidence reflector with a wideband, multilayer Mo/Si reflective coating. Also, the grating and first focusing element could be combined into one element that performs both spectral dispersion and focusing functions. For example, Figure 2 illustrates EUV source optics using a near-normal-incidence focusing mirror with a spectrum-dispersing phase-Fresnel diffraction grating formed on its surface. (A small, grazing-incidence diverging mirror near the focal plane expands the HHG source beam to fill the focusing mirror's aperture.)

In either the Figure 1 or Figure 2 configuration most of the IR power is separated from the filtered EUV harmonics at the focal plane. But aperture diffraction will spread a portion of the IR power into diffraction tails overlapping the EUV, so some additional filtering mechanism is required to remove the residual IR.

The IR diffraction tails could be mitigated by apodizing the grating aperture. Or the aperture shape can be designed to direct most of the aperture-diffracted IR away from the grating-diffracted EUV (e.g. by using a square aperture oriented at 45° to the grating lines). Also, the aperture size can be determined so that an IR diffraction null is centered on the EUV harmonics.

Another method for reducing the IR, which is detailed in this paper, is to superimpose the EUV-dispersing, phase-Fresnel grating on an IR-diffracting binary-optic structure, which creates a linear IR diffraction null ("nodal line") along the EUV foci.

Any of these methods could still leave a small but significant amount of IR in the filtered EUV beam. A zirconium filter can be used, if necessary, to substantially eliminate any residual IR. Zirconium IR-blocking filters typically have poor EUV transmittance (e.g. 20% [Ref. 1]). But if most of the IR has been eliminated by other means, then the zirconium filter can be a very thin element, which efficiently transmits EUV.

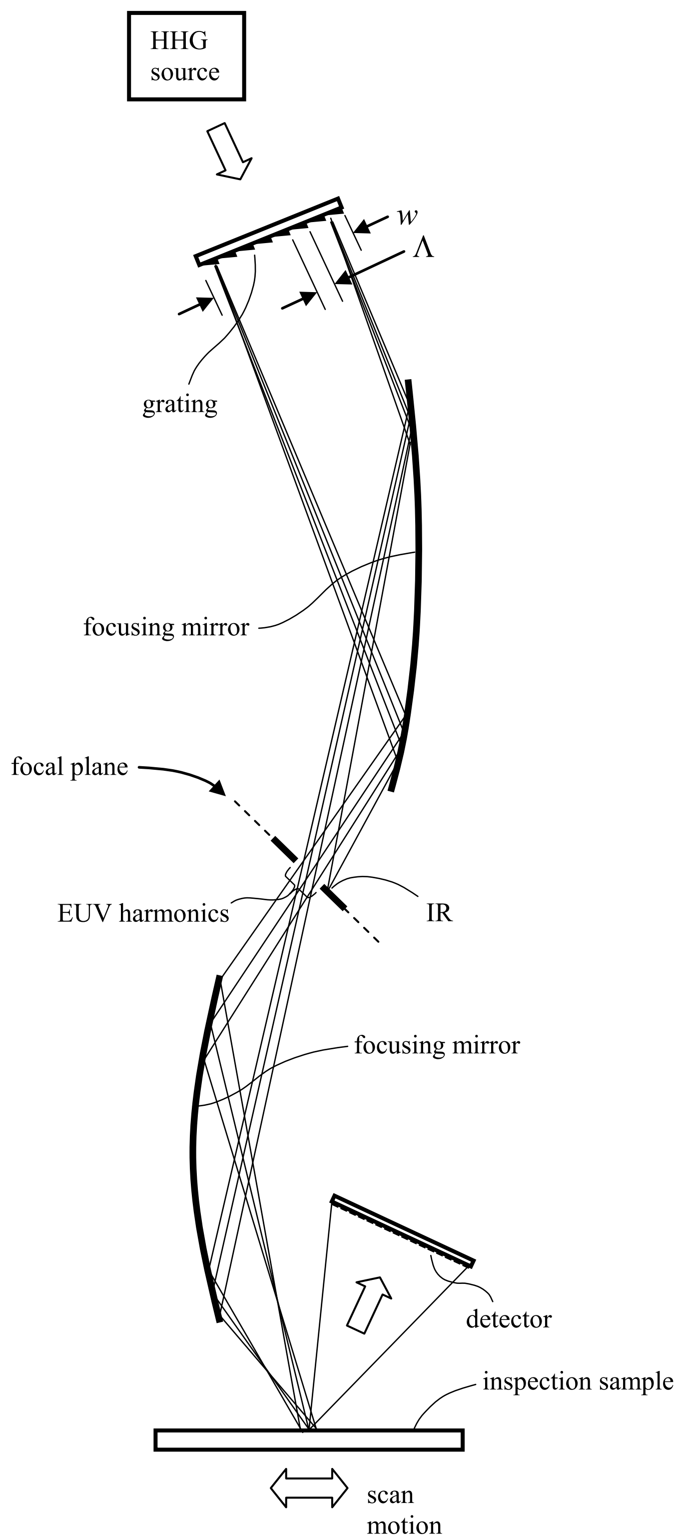

Figure 1. Multi-wavelength EUV microscope.

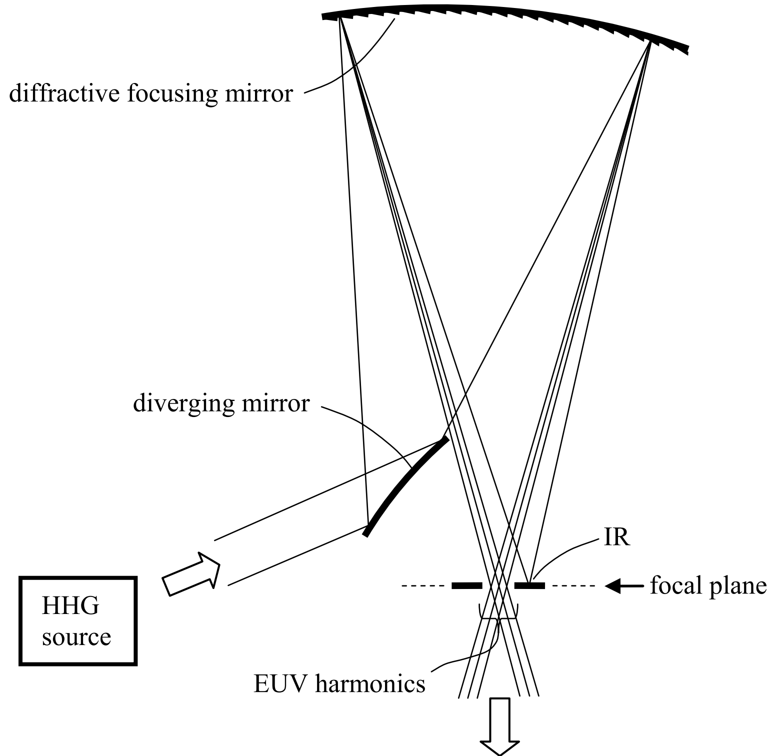

Figure 2. EUV source optics with near-normal-incidence, diffractive focusing mirror.

3. Phase-Fresnel Grating

A phase-Fresnel optic is a diffraction grating or grating-type surface with a sawtooth profile similar to a Fresnel lens, which preserves optical phase coherence between Fresnel facets at a particular "blaze" wavelength. [Ref. 5] An EUV phase-Fresnel grating can be a transmission element, e.g. comprising a molybdenum diffracting structure on a silicon substrate. [Ref. 6] Or it can be a reflective element, either a grazing-incident grating on a bare metal surface (e.g. ruthenium) or a near-normal-incidence element with a broadband multilayer reflecting coating (e.g., comprising Mo/Si bilayers). For the application of HHG spectral filtering, a near-normal-incidence reflector's limited spectral bandwidth could typically accommodate perhaps up to a dozen EUV harmonics [Ref. 7], whereas a phase-Fresnel transmission grating or grazing-incidence reflection grating can have good optical efficiency over a very wide spectral range covering many more harmonics. Phase-Fresnel gratings can be formed in silicon with atomic-scale dimensional accuracy. [Ref. 8]

The first-order diffraction efficiency η of a phase-Fresnel grating is approximately

$$\eta \approx \text{sinc}^2[\pi(\lambda_B / \lambda - 1)], \tag{1}$$

where λ_B is the blaze wavelength and $\text{sinc}[x] = \frac{\sin x}{x}$ (with $\text{sinc}[0] = 1$). This equation is based on Fourier-optics approximations, assuming small diffraction angles and near-normal incidence. η is a "relative efficiency" factor, which neglects transmission loss factors that are unrelated to grating diffraction. For example, a molybdenum EUV transmission grating on a silicon substrate

would have another efficiency factor of approximately 0.6 for the molybdenum transmittance, and a factor in the range of 0.8 to 0.9 for the silicon transmittance. An EUV reflection grating with a multilayer reflective coating would have a band-limited efficiency characteristic, which is not included in η.

The wideband efficiency characteristic defined by Eq. (1) can accommodate multiple EUV harmonics from an HHG source comprising a fundamental IR laser wavelength λ_1 and harmonic wavelengths λ_m, where

$$\lambda_m = \lambda_1 / m \quad (m \text{ odd}). \tag{2}$$

For example, the EUV microscope in Ref. 1 uses laser wavelength λ_1 = 800 nm and extracts a single harmonic λ_{59} = 13.56 nm. With a blaze wavelength $\lambda_B = \lambda_{59}$, a phase-Fresnel grating would exhibit the following relative efficiencies for nearby harmonics:

m	λ_m (nm)	η
55	14.55	98.5%
57	14.04	99.6%
59	13.56	100%
61	13.11	99.6%
63	12.70	98.5%

Again assuming small diffraction angles and near-normal incidence, the grating diverts the first diffraction order at wavelength λ by an angle of approximately λ / Λ relative to the zero order, where Λ is the grating period (Figure 1). Aperture diffraction will spread the diffracted beam over an angular range of approximately λ / w, where w is the width of the grating aperture. (It is assumed that the grating is the limiting aperture, as illustrated in Figure 1.) The difference in diffraction angles (λ / Λ) between successive odd-numbered harmonics (orders m and $m+2$) must be larger than the aperture-diffraction beam spread (λ / w) in order to separate the harmonics:

$$\lambda_m / \Lambda - \lambda_{m+2} / \Lambda > \lambda_m / w. \tag{3}$$

With substitution from Eq. (2), this implies that the number of grating facets (w / Λ) should be greater than half the harmonic order number (m),

$$w / \Lambda > \tfrac{1}{2} m. \tag{4}$$

(For example, with an aperture width w = 0.5 mm, IR wavelength λ_1 = 800 nm, and m = 59, the grating period Λ is less than $2w/m = 17\,\mu\text{m}$, the diffraction angle λ_m / Λ is greater than 0.8 mrad, and the angular separation between odd harmonics is at least 27 μrad.)

Any diffraction of the IR by the EUV-dispersing grating will be too widely scattered and too weak to be of any consequence. But the transmitted IR beam will be angularly dispersed by aperture diffraction, with most of the IR energy contained within a dispersion full angle of approximately λ_1 / w. The EUV diffraction angle λ_m / Λ should be large in relation to the IR dispersion half-angle to achieve separation of the EUV from most of the IR power,

$$\lambda_m / \Lambda > \tfrac{1}{2} \lambda_1 / w. \tag{5}$$

Again, this implies that $w / \Lambda > \frac{1}{2} m$ (Eq. (4)). However, this condition will not ensure separation of the EUV from the IR diffraction tails. The phase-Fresnel grating can be superimposed on an IR-masking structure, as described in section 4, to substantially eliminate the IR including the diffraction tails.

4. IR-Masking Structure for a Transmission Grating

Figure 3 illustrates an IR-masking structure, or "IR mask", which is a binary optic element comprising one or more lamellar lines crossing the grating aperture. The IR mask can be formed in silicon, and the EUV-dispersing, phase-Fresnel grating can be formed in molybdenum on top of the IR mask. (The grating is a transmission element in this design.) The grating and mask have orthogonal lines, and the IR mask induces some slight angular dispersion in the IR transmission in a direction orthogonal to the EUV dispersion.

The grating has a rectangular aperture with dimensions indicated in Figure 3 as w (in the EUV dispersion direction) and w' (in the IR dispersion direction). The binary optic's height dimension h is defined to induce a half-cycle (i.e., π-radian) optical phase shift across the mask steps at the IR wavelength λ_1:

$$h = \frac{\lambda_1}{2(n-1)}, \tag{6}$$

where n is the silicon refractive index at λ_1 (e.g. n=3.69 and h=149 nm at λ_1=800 nm). The IR mask lines cover half of the aperture area, resulting in an IR diffraction null along the EUV dispersion line on the focal plane in Figure 1.

These dimensional specifications assume small diffraction angles, near-normal incidence, and uniform illumination of the grating aperture. Also, surface reflections on the bottom silicon surface in Figure 3 are neglected. The height h and line area fraction can be determined more accurately to take these factors into account. Also, the following description can be generalized for nonuniform gratings on curved substrates (such as the diffractive mirror in Figure 2), for example, by applying the Huygens-Fresnel principle described in Ref. 4.

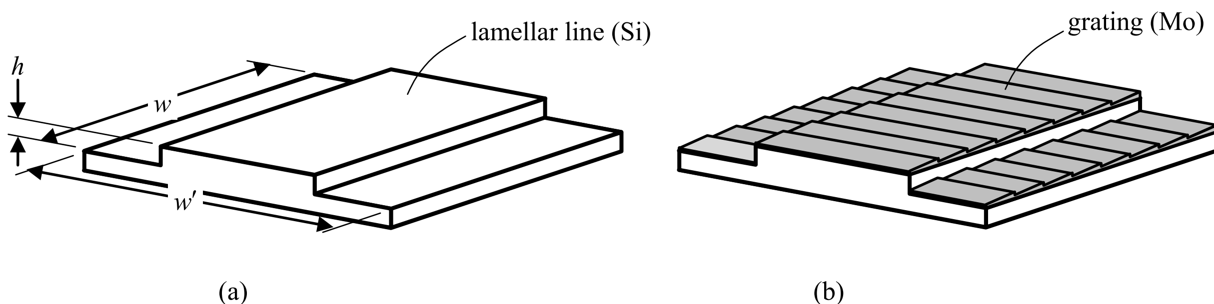

Figure 3. IR-masking structure (a) without and (b) with the superimposed EUV-dispersing grating.

Figure 4 illustrates several possible IR mask cross-section geometries (left column) and corresponding angular amplitude distributions of the transmitted IR beam (amplitude A versus diffraction angle θ, right column). The right-hand plots can be interpreted as cross-sections of the IR amplitude point-spread functions on the focal plane in Figure 1, along the IR dispersion direction. (The angle coordinate θ is multiplied by the focusing element's focal length to convert it to an approximate focal-plane coordinate position.) The point-spread cross-sections vary in amplitude, but not in shape, along the transverse EUV dispersion direction, and the IR null covers a nodal line perpendicular to the plane of Figure 4. The dispersed EUV harmonics are arrayed along the nodal line.

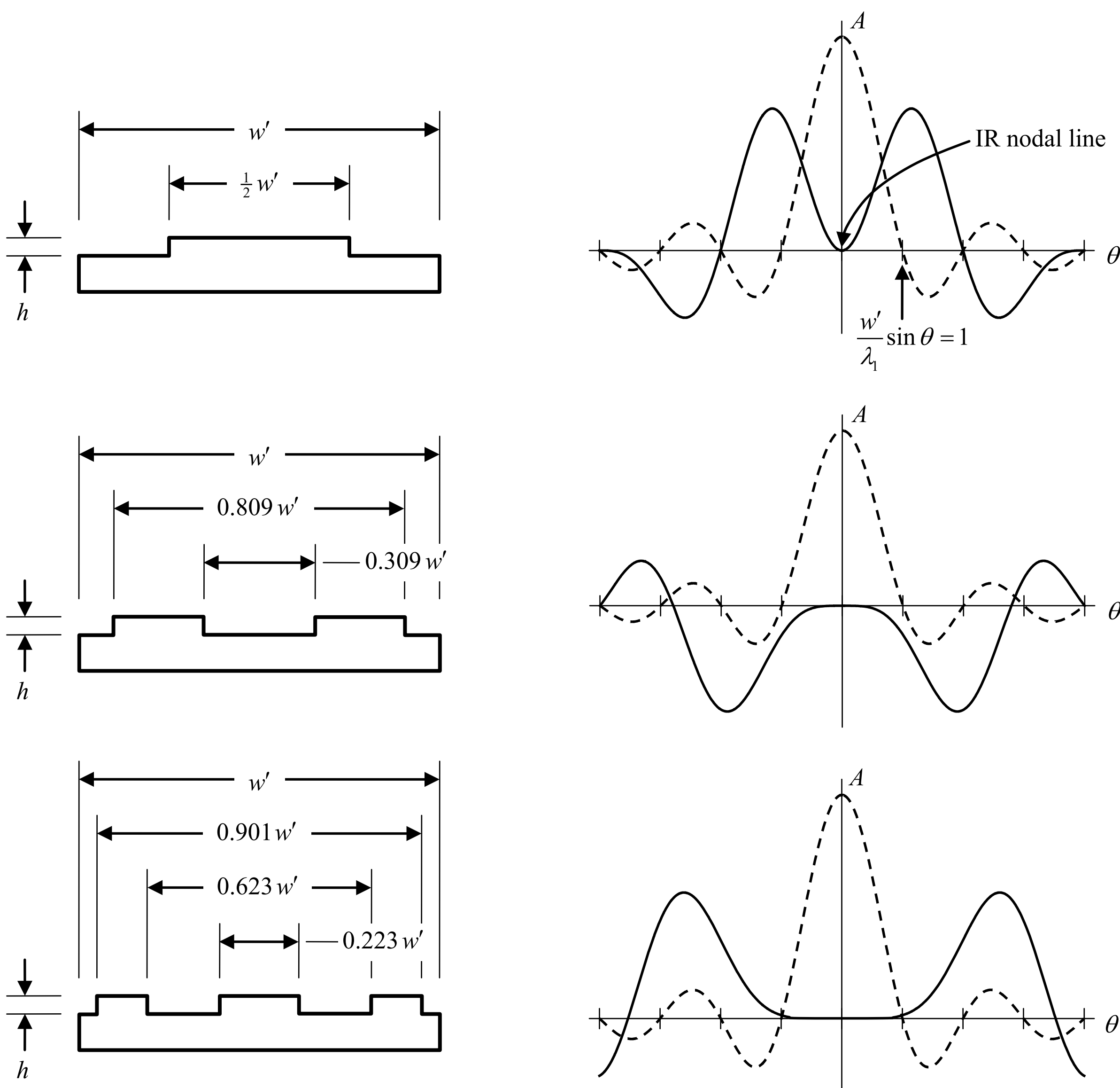

Figure 4. IR mask cross-sections (left column) and corresponding angular amplitude distributions (right column). The dashed plots represent the open-aperture diffraction pattern with no IR mask.

The dashed plots in Figure 4 represent the diffraction-limited point-spread function for an aperture of width w' with no IR mask. The first, second, and third rows in Figure 4 represent IR mask designs with one, two, or three mask lines, respectively. In each case the mask profile has even symmetry about the mask center line. The advantage of this symmetry condition is that not only will the diffraction amplitude be zero on the nodal line, but all odd-order derivatives of A versus θ will also be zero. The line edge locations of the one-line, two-line, and three-line designs are selected to also make all derivatives up to orders two, four, or six, respectively, equal to zero on the nodal line. Similar designs with more than three lines can be constructed to zero out higher-order derivatives.[1]

The IR mask's surface discontinuities can also affect the EUV harmonics, and the grating structure should be designed to minimize EUV dephasing across the mask steps. (Neglecting any such dephasing, the m-th harmonic λ_m has an amplitude point-spread function similar to the dashed plots in Figure 4, but narrower by a factor of m.) For EUV wavelengths near 13.5 nm the Si refractive index is very close to 1 and the optical phase discontinuity is negligible. But the EUV dephasing could be much more significant at other wavelengths. For example, at a 30-nm wavelength the silicon refractive index is 0.93 and the dephasing – without any design correction – would be 0.35 cycle. However, the top- and bottom-surface phase-Fresnel gratings can be designed with a lateral positioning offset to cancel out the phase discontinuity, at least for one particular EUV design wavelength.

Due to the slight EUV absorption by silicon, the IR mask's transmittance through the top surfaces will be lower than the bottom-surface transmittance (e.g., by a factor of 0.88 at 13.5 nm). This difference would probably not significantly affect the point-spread function, but the base thickness of the bottom-surface Mo grating can be increased to eliminate the IR transmittance discontinuity at a particular EUV design wavelength.

The grating phase offset and bottom-surface Mo thickness can be selected to eliminate any significant influence of the IR mask on one EUV wavelength, and to at least approximately eliminate the influence on nearby wavelengths. But there may be a limit to how many EUV harmonics can be used without incurring significant dephasing of the EUV beams by the IR

---

[1] These designs are based on the following equation defining the far-field amplitude A as a function of θ, given the mask's near-field amplitude A' as a function of the center-offset coordinate x on the mask.

$$A[\theta] = \frac{1}{w'} \int_{-w'/2}^{w'/2} A'[x] \exp[-i\,2\pi\,(x/\lambda_1)\sin\theta]\,dx$$

A' is +1 on the IR mask's top surfaces, and is -1 on the bottom surfaces. The horizontal axes in the right-hand column of Figure 4 are marked in units of $(w'/\lambda_1)\sin\theta$. The line edge locations are determined by the condition

$$\frac{1}{w'} \int_{-w'/2}^{w'/2} x^k\, A'[x]\,dx$$

for $k = 0, 1, \ldots, K-1$, where K is the number of edges. (As a result of the even-symmetry constraint, this condition is automatically satisfied for odd k.)

mask. A much wider range of EUV wavelengths might be usable with a reflective grating, as discussed in section 5.

5. IR-Masking Structure for a Reflection Grating, Near-Normal Incidence

The following discussion pertains to near-normal-incidence reflection gratings. Oblique-incidence gratings (including grazing-incidence reflection gratings) will be discussed in section 6.

Figures 3 and 4 are applicable to reflection gratings, except that in Figure 3 the structure need not be composed of silicon and molybdenum, and the grating is covered by a reflective film (e.g. a multilayer Mo/Si coating). The mask height dimension h in Figure 3 is

$$h = \frac{\lambda_1}{4}. \tag{7}$$

This induces a half-cycle optical phase shift across the mask steps at the IR wavelength λ_1. At EUV wavelength $\lambda_m = \lambda_1 / m$ the phase shift p_m (in cycle units) is

$$p_m = 2h / \lambda_m = \tfrac{1}{2} m. \tag{8}$$

(from Eq's. (2) and (7)). For m odd, the integer part of p_m is $\tfrac{1}{2}(m-1)$. EUV dephasing is only affected by the fractional part of p_m, which is

$$p_m \bmod 1 = p_m - \tfrac{1}{2}(m-1) = \tfrac{1}{2}. \tag{9}$$

Thus, the IR mask would induce a half-cycle phase shift across the mask steps in all EUV harmonics, resulting in complete dephasing of the harmonics. However, the dephasing can be eliminated – for all EUV harmonics – by phase-shifting the lower grating by a half cycle relative to the upper grating, as illustrated in Figure 5. The h-step phase shift p_m, plus the grating-induced phase shift, at wavelength λ_m is $\tfrac{1}{2} m + \tfrac{1}{2}$, which is integer-valued for m odd. Thus, assuming small diffraction angles and near-normal incidence, the IR mask would not result in dephasing at any of the harmonic wavelengths.

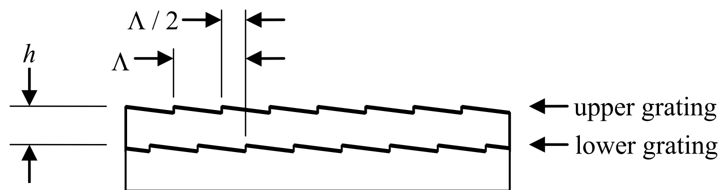

Figure 5. Side view of reflective IR mask with half-cycle phase shift between lower and upper gratings.

6. IR-Masking Structure for a Reflection Grating, Oblique Incidence

For oblique incidence (e.g., grazing incidence) of a plane wave on a horizontal diffraction grating, the optical phase shift associated with traversal of the incident beam across an empty vertical space of height h is $(h / \lambda)\cos\theta$ (in cycle units), where λ is the wavelength and θ is the incidence angle. A diffractively reflected beam (either the zero order or any diffraction

order) will similarly undergo a phase shift of $(h/\lambda)\cos\theta'$ in traversing the gap, where θ' is the diffraction angle (which is equal to θ for the zero order).

Figure 6 illustrates the diffraction geometry for a reflective IR mask with oblique incidence. The mask's height-h step induces a total phase offset of $(h/\lambda)(\cos\theta+\cos\theta')$ in the portion of the beam reflected off the bottom mask surface relative to the top-surface reflection. For the IR wavelength λ_1, only the zero-order reflected beam is of consequence, $\theta'=\theta$, and the step height h is determined so that the phase offset is one-half cycle:

$$(h/\lambda_1)2\cos\theta=\tfrac{1}{2};\;\; h=\frac{\lambda_1}{4\cos\theta}. \tag{10}$$

For a harmonic wavelength λ_m the step-induced phase shift p_m is

$$p_m=(h/\lambda_m)(\cos\theta+\cos\theta')=\tfrac{1}{4}m\left(1+\frac{\cos\theta'}{\cos\theta}\right). \tag{11}$$

(from Eq's. (10) and (2)). If the diffractive scattering angles do not deviate much from the zero order then θ' is close to θ and the phase shift is approximately $\tfrac{1}{2}m$, as in the near-normal-incidence case (Eq. (8)). Otherwise, the phase offset between the top and bottom gratings can be defined to eliminate EUV dephasing at least for a particular diffraction angle θ'. Even if θ' deviates significantly from θ, good phase coherence can be maintained if there is minimal variation of $\cos\theta'$ over a broad range of harmonics. A procedure for calculating $\cos\theta'$ for each harmonic is outlined below.

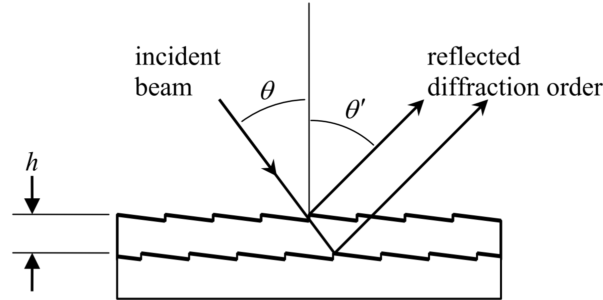

Figure 6. Oblique-incidence diffraction geometry for a reflective IR mask.

Figure 7 illustrates the diffraction geometry for conical diffraction from a phase-Fresnel reflection grating. The "$\hat{u}$" vectors represent ray direction vectors, which are defined by their projections onto orthogonal coordinate basis vectors $\hat{e}_1$, $\hat{e}_2$, and $\hat{e}_3$. $\hat{e}_1$ is perpendicular to the grating substrate. $\hat{e}_2$ is parallel to the substrate and perpendicular to the grating lines, and points in the direction opposite to the Fresnel facets' profile gradient. $\hat{e}_3$ is parallel to the grating lines. The direction vectors $\hat{u}$ are unit vectors ($|\hat{u}|=1$), and for a particular reflected beam with direction vector $\hat{u}$ the $\cos\theta'$ factor in Eq. (11) is the $\hat{e}_1$ projection of $\hat{u}$,

$$\cos\theta'=\hat{e}_1\bullet\hat{u}\,. \tag{12}$$

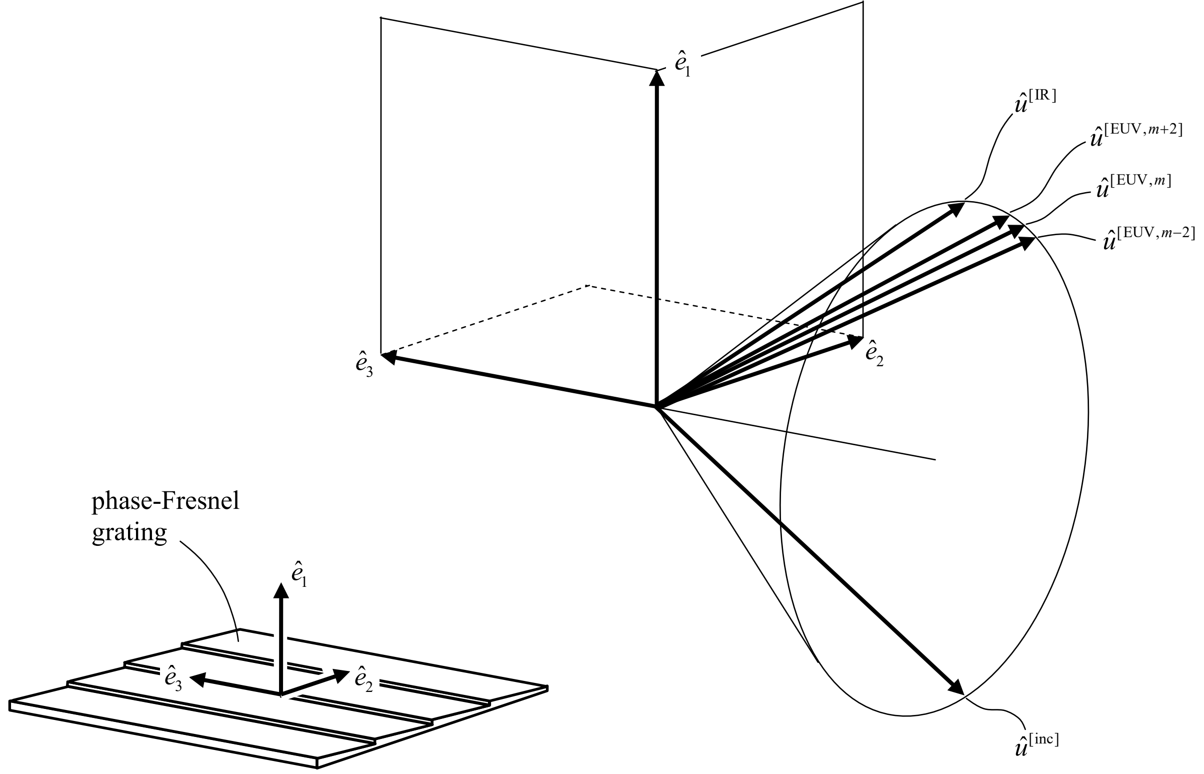

Figure 7. Conical diffraction geometry for a reflection grating.

The incident beam direction is defined by unit vector $\hat{u}^{[\mathrm{inc}]}$; the reflected (zero-order) IR beam has unit direction vector $\hat{u}^{[\mathrm{IR}]}$, and the order-m harmonic (first-order diffracted beam at wavelength λ_m) has unit direction vector $\hat{u}^{[\mathrm{EUV},\,m]}$ (Figure 7). The $\hat{e}_1$ projection of $\hat{u}^{[\mathrm{inc}]}$ is negative, hence

$$\cos\theta = -\hat{e}_1 \bullet \hat{u}^{[\mathrm{inc}]} . \tag{13}$$

The direction vectors are all arrayed along a cone with a common $\hat{e}_3$ projection,

$$\hat{e}_3 \bullet \hat{u}^{[\mathrm{inc}]} = \hat{e}_3 \bullet \hat{u}^{[\mathrm{IR}]} = \hat{e}_3 \bullet \hat{u}^{[\mathrm{EUV},\,m]} . \tag{14}$$

(If the incident direction $\hat{u}^{[\mathrm{inc}]}$ is perpendicular to the grating lines, then the cone degenerates to a plane.) $\hat{u}^{[\mathrm{IR}]}$ and $\hat{u}^{[\mathrm{inc}]}$ differ only in the sign of their $\hat{e}_1$ projections,

$$\hat{e}_1 \bullet \hat{u}^{[\mathrm{IR}]} = -\hat{e}_1 \bullet \hat{u}^{[\mathrm{inc}]} , \quad \hat{e}_2 \bullet \hat{u}^{[\mathrm{IR}]} = \hat{e}_2 \bullet \hat{u}^{[\mathrm{inc}]} . \tag{15}$$

The $\hat{e}_2$ projection of $\hat{u}^{[\mathrm{EUV},\,m]}$ has the following relationship to the incident beam direction,

$$\hat{e}_2 \bullet \hat{u}^{[\mathrm{EUV},\,m]} = \hat{e}_2 \bullet \hat{u}^{[\mathrm{inc}]} + \lambda_m / \Lambda . \tag{16}$$

The $\hat{e}_1$ projection of $\hat{u}^{[\mathrm{EUV},\,m]}$ is obtained from its $\hat{e}_2$ and $\hat{e}_3$ projections and the condition that $\hat{u}^{[\mathrm{EUV},\,m]}$ is a unit vector,

$$\hat{e}_1 \bullet \hat{u}^{[\mathrm{EUV},\,m]} = \sqrt{1 - (\hat{e}_2 \bullet \hat{u}^{[\mathrm{EUV},\,m]})^2 - (\hat{e}_3 \bullet \hat{u}^{[\mathrm{EUV},\,m]})^2} . \tag{17}$$

Eq's. (14)-(17) define $\hat{u}^{[\mathrm{IR}]}$ and $\hat{u}^{[\mathrm{EUV},\,m]}$ from $\hat{u}^{[\mathrm{inc}]}$.

Eq. (17) defines the $\cos\theta'$ factor for harmonic m (cf. Eq. (12)),

$$\cos\theta' = \hat{e}_1 \bullet \hat{u}^{[\mathrm{EUV},\,m]} . \tag{18}$$

(The m dependence of $\cos\theta'$ is implicit.) Substituting Eq's. (16) and (14) in Eq. (17), applying the relation $1-(\hat{e}_3\bullet\hat{u}^{[\mathrm{inc}]})^2 = (\hat{e}_1\bullet\hat{u}^{[\mathrm{inc}]})^2 + (\hat{e}_2\bullet\hat{u}^{[\mathrm{inc}]})^2$ (because $\hat{u}^{[\mathrm{inc}]}$ is a unit vector), and substituting Eq. (13), the following result is obtained,

$$\cos\theta' = \sqrt{\cos^2\theta - (\lambda_m/\Lambda + 2\,\hat{e}_2\bullet\hat{u}^{[\mathrm{inc}]})\,\lambda_m/\Lambda} . \tag{19}$$

Eq. (19) is substituted in Eq. (11),

$$p_m = \tfrac{1}{4} m \left(1 + \frac{\sqrt{\cos^2\theta - (\lambda_m/\Lambda + 2\,\hat{e}_2\bullet\hat{u}^{[\mathrm{inc}]})\,\lambda_m/\Lambda}}{\cos\theta} \right). \tag{20}$$

Typically, the λ_m/Λ factor in Eq. (20) is much smaller than $\cos^2\theta$ and the above equation can be approximated as

$$p_m \approx \tfrac{1}{2} m \left(1 - \frac{(\lambda_m/\Lambda + 2\,\hat{e}_2\bullet\hat{u}^{[\mathrm{inc}]})\,\lambda_m/\Lambda}{4\cos^2\theta} \right) \quad (\lambda_m/\Lambda << \cos^2\theta) . \tag{21}$$

This is approximately equal to $\tfrac{1}{2}m$ (as in Eq. (8)), and the fractional part of p_m is

$$p_m \bmod 1 = p_m - \tfrac{1}{2}(m-1) \approx \tfrac{1}{2} - m\frac{(\lambda_m/\Lambda + 2\,\hat{e}_2\bullet\hat{u}^{[\mathrm{inc}]})\,\lambda_m/\Lambda}{8\cos^2\theta} . \tag{22}$$

Substituting $\lambda_m = \lambda_1/m$ (Eq. (2)), this becomes

$$p_m \bmod 1 \approx \tfrac{1}{2} - \frac{(\lambda_1/(m\Lambda) + 2\,\hat{e}_2\bullet\hat{u}^{[\mathrm{inc}]})\,\lambda_1/\Lambda}{8\cos^2\theta} . \tag{23}$$

The grating phase can offset the step-induced phase shift p_m as illustrated in Figure 5, except that the offset is not exactly one-half cycle. The bottom grating phase offset is specified as $-(p_m \bmod 1)$ for one particular harmonic index m, resulting in no EUV dephasing at that harmonic and only very minimal dephasing at nearby harmonics. The offset is implemented by positionally translating the bottom grating relative to the top grating by $(p_m \bmod 1)\Lambda$ in the direction opposite the grating profile gradient, i.e. to the right in Figure 5.

The $\hat{e}_2\bullet\hat{u}^{[\mathrm{inc}]}$ term in Eq. (23) only induces a constant (m-independent) change in $p_m \bmod 1$, which will be completely neutralized by the grating phase offset. The incident beam direction only affects EUV dephasing through the denominator factor $\cos^2\theta$ in Eq. (23).

Once the diffraction geometry is defined, the grating can be blazed for maximum diffraction efficiency at a particular wavelength λ_m by making the Fresnel facet surfaces orthogonal to the vector $\hat{u}^{[\mathrm{EUV},\,m]} - \hat{u}^{[\mathrm{inc}]}$. (The facets behave as geometric-optics mirrors at the blaze wavelength.)

References

1. Naulleau, Patrick P., Christopher N. Anderson, Erik H. Anderson, Nord Andreson, Weilun Chao, Changhoon Choi, Kenneth A. Goldberg et al. "Electro-optical system for scanning microscopy of extreme ultraviolet masks with a high harmonic generation source." *Optics express* 22, no. 17 (2014): 20144-20154.
http://dx.doi.org/10.1364/OE.22.020144

2. Zhang, Bosheng, Daniel E. Adams, Matthew D. Seaberg, Dennis F. Gardner, Elisabeth R. Shanblatt, Henry Kapteyn, and Margaret Murnane. "Quantitative tabletop coherent diffraction imaging microscope for EUV lithography mask inspection." In *SPIE Advanced Lithography*, pp. 90501D-90501D. International Society for Optics and Photonics, 2014.
http://dx.doi.org/10.1117/12.2046526

3. Karl, Robert, Charles Bevis, Raymond Lopez-Rios, Jonathan Reichanadter, Dennis Gardner, Christina Porter, Elisabeth Shanblatt et al. "Spatial, spectral, and polarization multiplexed ptychography." *Optics Express* 23, no. 23 (2015): 30250-30258.
http://dx.doi.org/10.1364/OE.23.030250

4. Raimondi, L., and D. Spiga. "Point spread function of real Wolter-I X-ray mirrors: computation by means of the Huygens-Fresnel principle." In *SPIE Optical Engineering+ Applications*, pp. 81470Z-81470Z. International Society for Optics and Photonics, 2011.
http://dx.doi.org/10.1117/12.895321

5. Miyamoto, Kenro. "The phase Fresnel lens." *JOSA* 51, no. 1 (1961): 17-20.
http://dx.doi.org/10.1364/JOSA.51.000017

6. Johnson, Kenneth C. "Scanned-spot-array extreme ultraviolet imaging for high-volume maskless lithography." *Journal of Vacuum Science & Technology B* 30, no. 5 (2012): 051606.
http://dx.doi.org/10.1116/1.4752112

7. Aquila, A. L., F. Salmassi, F. Dollar, Y. Liu, and E. Gullikson. "Developments in realistic design for aperiodic Mo/Si multilayer mirrors." *Optics express* 14, no. 21 (2006): 10073-10078.
http://dx.doi.org/10.1364/OE.14.010073

8. Voronov, D. L., E. H. Anderson, R. Cambie, Peter Gawlitza, L. I. Goray, E. M. Gullikson, F. Salmassi, T. Warwick, V. V. Yashchuk, and H. A. Padmore. "Development of near atomically perfect diffraction gratings for EUV and soft x-rays with very high efficiency and resolving power." In *Journal of Physics: Conference Series*, vol. 425, no. 15, p. 152006. IOP Publishing, 2013.
http://dx.doi.org/10.1088/1742-6596/425/15/152006